

## Pressure-induced metal–insulator transitions in chalcogenide $\text{NiS}_{2-x}\text{Se}_x$

Tayyaba Hussain<sup>a</sup>, Myeong-jun Oh<sup>a</sup>, Muhammad Nauman<sup>a</sup>, Younjung Jo<sup>a,\*</sup>, Garam Han<sup>b</sup>,  
Changyoung Kim<sup>b</sup>, Woun Kang<sup>c</sup>

<sup>a</sup> Department of Physics, Kyungpook National University, Daegu 41566, South Korea

<sup>b</sup> Center for Correlated Electron Systems, Institute of Basic Science, Seoul 08826, South Korea

<sup>c</sup> Department of Physics, Ewha Womans University, Seoul 03760, South Korea

### ARTICLE INFO

#### Keywords:

$\text{NiS}_{1.9}\text{Se}_{0.1}$   
 $\rho(T)$  measurements  
Magnetic measurements  
Metal–insulator transition (MIT)  
Magnetic phase transition  
Non-Fermi-liquid behavior

### ABSTRACT

We report the temperature-dependent resistivity  $\rho(T)$  of chalcogenide  $\text{NiS}_{2-x}\text{Se}_x$  ( $x = 0.1$ ) using hydrostatic pressure as a control parameter in the temperature range of 4–300 K. The insulating behavior of  $\rho(T)$  survives at low temperatures in the pressure regime below 7.5 kbar, whereas a clear insulator-to-metallic transition is observed above 7.5 kbar. Two types of magnetic transitions, from the paramagnetic (PM) to the antiferromagnetic (AFM) state and from the AFM state to the weak ferromagnetic (WF) state, were evaluated and confirmed by magnetization measurement. According to the temperature–pressure phase diagram, the WF phase survives up to 7.5 kbar, and the transition temperature of the WF transition decreases as the pressure increases, whereas the metal–insulator transition temperature increases up to 9.4 kbar. We analyzed the metallic behavior and proposed Fermi-liquid behavior of  $\text{NiS}_{1.9}\text{Se}_{0.1}$ .

### 1. Introduction

The understanding of strongly correlated phenomena, particularly through the metal–insulator transition (MIT), has received constant attention in recent decades [1]. In particular, the MIT in *d*-electron systems (i.e., transition-metal compounds) is more rigorous and systematic [2]. The MIT can be controlled by changing the temperature, pressure, and carrier concentration [3] to induce a drastic change in the physical properties. According to the local density approximation, the MIT is caused primarily by three basic parameters: the Coulomb repulsion  $U$ , charge transfer interval  $\Delta$ , and bandwidth  $W$ . The hydrostatic pressure increases the  $W/U$  ratio and induces the MIT. In contrast, chemical pressure reduces the  $W/\Delta$  ratio, which also causes the MIT [4,5]. This has generated interest in the study of the chalcogenide  $\text{NiS}_{2-x}\text{Se}_x$  system. The cubic pyrite  $\text{NiS}_2$  crystal has long been identified as a canonical Mott–Hubbard correlated insulator [6–11]; the  $3p$  band of S and the Ni  $t_{2g}$  band are significantly below the semicharged Ni  $e_g$  band, which is responsible for the on-site Coulomb repulsion of S, resulting in an insulating energy gap  $E_g$  of  $\sim 1$ –10 meV and an emerging Mott insulator with an  $e_g$  bandwidth  $W$  of 2.1 eV [12]. Paramagnetic (PM)  $\text{NiS}_2$  at room temperature is aligned antiferromagnetically below  $\sim 38$  K, and the compound is arranged ferromagnetically when the second transition occurs below 30 K [13,14]. The Mott insulating gap in  $\text{NiS}_{2-x}\text{Se}_x$  can be suppressed by varying the temperature  $T$ , Se content  $x$ , or hydrostatic pressure  $P$  [15]. According to the

phase diagram of  $\text{NiS}_{2-x}\text{Se}_x$ , the MIT resulting from chemical pressure was obtained at  $x \sim 0.5$  at room temperature, whereas the magnetic transitions to an antiferromagnetic (AFM) metal and from an AFM metal to a PM metal were obtained at  $x \sim 0.4$  and  $x \sim 1$ , respectively [7,16]. The hydrostatic-pressure-driven MIT was also discussed in previous reports [6,15,17,18]. In the pure pyrite  $\text{NiS}_2$  compound, the MIT occurred at 30 kbar, whereas magnetic transitions from the weak ferromagnetic (WF) to the AFM phase at 26 kbar [15] and from the AFM to the PM phase at 70 kbar [16] were observed. For doped  $\text{NiS}_{2-x}\text{Se}_x$  ( $x = 0.4$ ), the MIT appeared at  $\sim 1.6$  kbar [17]. It has been observed that the external pressure closes a band gap associated with the flexibility of the Se–Se bond length; the Se–Se bond expands under pressure, but the S–S bond length remains constant [5].

The  $\text{NiS}_{2-x}\text{Se}_x$  system exhibits two unique characteristics: first, it is a chalcogenide that exhibits an MIT between self-aligned phases [19]. Second, the parent compounds,  $\text{NiS}_2$  and  $\text{NiSe}_2$ , exhibit a weak first-order transition with a symmetric structure while maintaining an isocubic structure. However, their electronic characteristics are completely different; i.e.,  $\text{NiS}_2$  is a charge transfer insulator, and  $\text{NiSe}_2$  is a metal [20–24]. Therefore, the structure-independent MIT is suitable for investigating the electronic correlation that determines the metallic state of this system [5].

The MIT obtained by a high degree of chemical substitution of Se introduces impurities and alters physical parameters that cannot be controlled, whereas the pressure-induced MIT provides a more

\* Corresponding author.

E-mail address: [jophy@knu.ac.kr](mailto:jophy@knu.ac.kr) (Y. Jo).

<https://doi.org/10.1016/j.physb.2017.11.032>

Received 30 June 2017; Received in revised form 2 October 2017; Accepted 8 November 2017  
0921-4526/ © 2017 Elsevier B.V. All rights reserved.

systematic method of controlling the properties [25]. In this work, we studied the pressure-induced MIT for  $\text{NiS}_{2-x}\text{Se}_x$  with a low doping concentration ( $x = 0.1$ ). In  $\text{NiS}_{1.9}\text{Se}_{0.1}$ , the MIT is achieved at a lower pressure than in the pyrite compound  $\text{NiS}_2$ , so the MIT can be controlled using our Be–Cu pressure cell. At lower pressures, the resistivity of the sample increases with decreasing temperature and shows clear insulating behavior. The resistivity passes through a small maximum in the range of 30–80 K and decreases monotonically as the temperature is increased. At high pressures, the compound exhibits metallic behavior at low temperatures. We constructed the temperature–pressure phase diagram of  $\text{NiS}_{1.9}\text{Se}_{0.1}$ , where the WF phase survives up to 7.5 kbar, the transition temperature of the WF decreases as the pressure increases, and the MIT temperature increases up to 9.4 kbar. We also analyzed the metallic behavior and proposed Fermi liquid behavior (FL) at higher temperatures of  $\text{NiS}_{1.9}\text{Se}_{0.1}$ .

## 2. Experimental details

High-quality single crystals of  $\text{NiS}_{1.9}\text{Se}_{0.1}$  were grown using a well-known chemical vapor transport method. The stoichiometric composition of  $\text{NiS}_{2-x}\text{Se}_x$  was analyzed by an energy-dispersive x-ray spectroscopy (EDX), and the value of  $x$  was observed to be 0.104. The stoichiometry is slightly different for the sample position, but the difference is less than or equal to the error of the instrument. Therefore, it has a constant stoichiometry within a microscale. We applied hydrostatic pressure up to 10 kbar using a piston-type Be–Cu pressure cell. Lead and manganese wires were mounted together with the sample, and the resistivity of manganese and the superconducting transition temperature of lead were used to determine the pressure in the cell. The pressure coefficients are given by  $dR/dP = R_0 \sim 2.48 \Omega/\text{bar}$  for manganese and  $dT_c/dP = -3.61 \times 10^{-5} \text{ K}/\text{bar}$  for lead. Electrical transport measurements were performed under pressure in a four-probe configuration. We measured the temperature dependence of the resistivity of the crystals down to 4 K by using a closed-cycle refrigerator, and the applied current was  $\sim 1 \mu\text{A}$ . The temperature- and magnetic-field-dependent magnetizations were measured using a superconducting quantum interference device (Quantum Design, Inc., San Diego, CA, USA).

## 3. Results and discussion

Fig. 1(a) shows the susceptibility of  $\text{NiS}_{1.9}\text{Se}_{0.1}$  when a 0.1 T magnetic field is applied. Two types of magnetic ordering exist. The first transition, to the AFM regime, occurs at  $T_N \sim 40$  K, as shown in the inset in Fig. 1(a). A second transition, to the canted AFM state, occurs around  $T_{WF} \sim 25$  K. Because of the canting, a WF component develops below  $T_{WF}$  [26]. A comparison to pure  $\text{NiS}_2$  also shows the same transitions to the AFM and WF phases at 37 and 30 K, respectively. This result is consistent with those in previous reports [22,29]. The magnetic field ( $H$ ) dependence of the magnetization ( $M$ ) at 10 K is shown in Fig. 1(b); the  $M$ – $H$  loop exhibits ferromagnetic behavior, which confirms the dominance of the ferromagnetic contribution observed in the  $M$ – $T$  curve. As the magnetic field increases, the hysteresis disappears above 1.5 T; further, the magnetization gradually increases, but the saturation is not complete even at high magnetic fields. This implies a mixed state of weak ferromagnetism along with the AFM contribution.

The Mott insulator  $\text{NiS}_{2-x}\text{Se}_x$  ( $x = 0.1$ ) system can be transformed to the metallic state by applying an external pressure. At low pressures, the temperature-dependent resistivity  $\rho(T)$  shows clear insulating behavior, with a maximum value of  $\sim 4.6 \times 10^3 \Omega \text{ cm}$  at 4 K, as shown in Fig. 2(a), which is approximately the same order of magnitude as the value of  $\rho = 2.0 \times 10^3 \Omega \text{ cm}$  for  $x = 0.24$  [27]. The resistivity passes through a small local minimum between 20 and 40 K (arrows). This is referred to as the WF transition temperature ( $T_{WF}$ ), such as spin canting in the AFM state. In Fig. 2(b), a drastic change is observed at

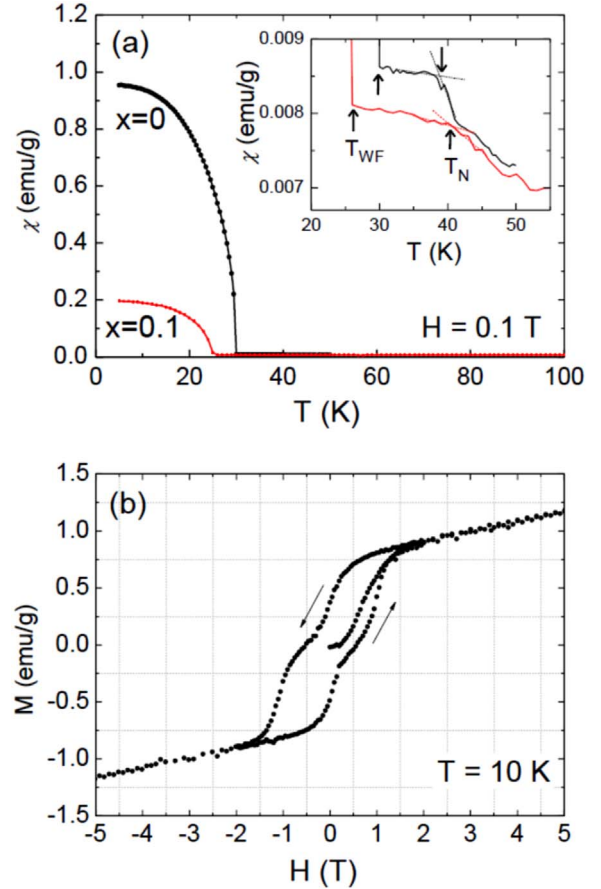


**Fig. 1.** (a) Temperature-dependent magnetization of  $\text{NiS}_2$  and  $\text{NiS}_{1.9}\text{Se}_{0.1}$  at 0.1 T showing the transitions to the AFM state around 40 K (inset) and to the WF ground state below  $T_{WF}$  at ambient pressure. (b) Magnetization of  $\text{NiS}_{1.9}\text{Se}_{0.1}$  at 10 K shows a hysteresis loop.

7.5 kbar, where the low-temperature resistivity decreases by many orders of magnitude, indicating the occurrence of MIT. During the MIT, the small steps in the resistivity curve indicate that, upon metallization, the volume shrinkage of successive parts of the sample influences the stress acting on the remaining sample [12,15]. Therefore, different parts of the sample experience the MIT at different temperatures, whereas the pressure homogeneity fully restores the metallic regime at low temperatures.

Fig. 3 shows the temperature–pressure ( $T$ – $P$ ) phase diagram of  $\text{NiS}_{1.9}\text{Se}_{0.1}$  constructed from the  $\rho(T)$  measurements in Fig. 2. The WF phase survives up to the pressure at which the MIT occurs and vanishes in the metallic phase.  $T_{WF}$  decreases as the pressure increases. The MIT occurs in the AFM state at high pressure, and the transition temperature  $T_{MIT}$  increases up to 9.4 kbar. It has been mentioned that  $T_{WF}$  decreases with doping, whereas in pure  $\text{NiS}_2$ , it increases linearly with pressure [25]. The origin of the WF ordering at low temperatures is still unclear. It was also mentioned that pure  $\text{NiS}_2$  shows a large entropy change at the WF transition, which is responsible for strong magnon–phonon interaction. It plays an important role in construction of the complicated spin canting structure [28]. We expect the same contribution at  $x = 0.1$ .

$\Delta\rho = \rho - \rho_0$  for high-pressure metallic parts above 7 kbar is plotted in Fig. 4(a). The insulator-to-metal transition is not shown.  $\rho_0$  is the residual resistivity inferred from extrapolation of the  $\rho(T)$  curve toward 0 K. It is apparent that the resistivity exhibits a dominant quadratic temperature dependence. We tried to fit  $\Delta\rho$  by a power law  $\Delta\rho(T) = AT^n$  and found the best fit for  $n$  value around 2.4. The resistivity data for different pressures plotted against  $T^{2.4}$  is shown in Fig. 4(b). The fitted values of the coefficient  $A$  as a function of pressure

Download English Version:

<https://daneshyari.com/en/article/8161123>

Download Persian Version:

<https://daneshyari.com/article/8161123>

[Daneshyari.com](https://daneshyari.com)